Chemical Geology 505 (2019) 66–75

Contents lists available at ScienceDirect

Chemical Geology

journal homepage: www.elsevier.com/locate/chemgeo

Pyrite sulfur isotopes constrained by sedimentation rates: Evidence from sediments on the East China Sea inner shelf since the late Pleistocene

Xiting Liu[a,b,*], David Fike[c], Anchun Li[d,**], Jiang Dong[d,e], Fangjian Xu[f], Guangchao Zhuang[g], Rebecca Rendle-Bühring[h], Shiming Wan[d]

[a] Key Laboratory of Submarine Geosciences and Prospecting Technology, College of Marine Geosciences, Ocean University of China, Qingdao 266100, China
[b] Laboratory for Marine Geology, Qingdao National Laboratory for Marine Science and Technology, Qingdao 266061, China
[c] Department of Earth and Planetary Sciences, Washington University, St. Louis, MO 63130, USA
[d] Key Laboratory of Marine Geology and Environment, Institute of Oceanology, Chinese Academy of Sciences, Qingdao 266071, China
[e] University of Chinese Academy of Sciences, Beijing 100049, China
[f] School of Geosciences, China University of Petroleum, Qingdao 266580, China
[g] Department of Marine Sciences, University of Georgia, Athens 30602, USA
[h] MARUM – Center for Marine Environmental Sciences, University of Bremen, Bremen D-28359, Germany

ARTICLE INFO

Editor: E. B Michael

Keywords:
Pyrite
Sulfur isotope
Microbial sulfate reduction
Mud depocenter
East China Sea

ABSTRACT

Isotopic compositions of coeval sulfide and sulfate have been widely employed to reconstruct the seawater chemistry evolution over geologic time; however, these signals can be modulated by other factors, such as the sedimentation rate. Here, we present a data set of pyrite sulfur isotopes ($\delta^{34}S_{py}$) derived from 60-m drilled core sediments deposited on the inner shelf of the East China Sea since 16.5 ka. The resulting $\delta^{34}S_{py}$ values range from −38.2 to 15.0‰ (Vienna Canyon Diablo Troilite; V-CDT), representing a range of 53.2‰. Freshwater deposition before 12.3 ka produced a limited pyrite abundance and $\delta^{34}S_{py}$ values that fall within the typical range of freshwater environments. After the marine incursion in the study area at 12.3 ka, variations in the $\delta^{34}S_{py}$ values become significantly correlated with sedimentation rates (SRs; $r = 0.78$, $p < 0.01$), which were controlled by the intensity of coastal currents in response to the East Asian winter monsoon. Specifically, pyrite sulfur is markedly depleted in ^{34}S during the intervals with low SRs ($\delta^{34}S_{py} < -30‰$) relative to that observed during the intervals with high SRs ($\delta^{34}S_{py} > 0‰$), suggesting that SRs exert controls on $\delta^{34}S_{py}$ values. We propose that these sedimentary controls are expressed by modulating the connectivity between porewaters and the overlying seawater. Low SRs tend to form an open diagenetic system, in which the pyrites are able to preserve the large biological fractionations associated with microbial sulfate reduction (and disproportionation). In contrast, high SRs favour a restricted diagenetic system, in which the distillation of porewater sulfate produces pyrites enriched in ^{34}S, masking the magnitude of biological fractionation during microbial sulfur cycling. These findings highlight the critical effect of the local sedimentation regime on pyrite sulfur isotopic compositions, especially within shallow depositional environments, over geologic time.

1. Introduction

The burial of sedimentary pyrite in marine sediments has played a primary role in controlling the oxygen concentration in the atmosphere and the sulfate concentration in seawater over the Phanerozoic eon (Berner, 1984; Canfield, 2001a; Fike et al., 2015). The abundance and isotopic compositions of sulfide and coeval sulfate minerals in the sedimentary record have been widely used to reconstruct the sulfur cycle and to indicate the evolution of the ocean-atmosphere system over geologic time (Canfield et al., 2000; Loyd et al., 2012; Jones and Fike, 2013; Algeo et al., 2015; Kunzmann et al., 2017). Along continental margins, microbial sulfate reduction (MSR) is believed to be the dominant pathway that produces sulfur isotopic fractionation between sulfide and sulfate (Jørgensen, 1982; Canfield, 2001a). During MSR, $^{32}SO_4^{2-}$ is preferentially utilized relative to $^{34}SO_4^{2-}$, resulting in the release of ^{34}S-depleted sulfide. The magnitude of sulfur isotopic

* Correspondence to: X. Liu, Key Laboratory of Submarine Geosciences and Prospecting Technology, College of Marine Geosciences, Ocean University of China, Qingdao 266100, China.
** Corresponding author.
E-mail addresses: liuxiting@ouc.edu.cn (X. Liu), acli@qdio.ac.cn (A. Li).

https://doi.org/10.1016/j.chemgeo.2018.12.014
Received 2 July 2018; Received in revised form 11 December 2018; Accepted 17 December 2018
Available online 19 December 2018
0009-2541/

fractionation during MSR was considered to be no > 46‰ (e.g., Kaplan and Rittenberg, 1964; Rees, 1973). However, recent studies have found that sulfur isotopic fractionation could be much higher than 46‰ and reach up to 70‰ (e.g., Canfield et al., 2010; Sim et al., 2011a; Wortmann et al., 2001). The magnitude of such isotopic fractionation between sulfide and sulfate is a function of physiology, which depends on both biochemical and environmental factors (Canfield, 2001b; Sim et al., 2011b; Leavitt et al., 2013; Wing and Halevy, 2014; Gomes and Hurtgen, 2015). In addition, the abundance and isotopic composition of sulfide can be influenced by other factors, such as the depositional environment (Wilkin and Arthur, 2001), isotopic exchange between different reservoirs (Jørgensen et al., 2004), hydrodynamics and bioturbation processes (Aller et al., 2010), organic carbon preserved in sediment (Leavitt et al., 2013), and sediment reworking (Riedinger et al., 2017). Thus, to interpret sulfur isotopic signals in geological records, it is necessary to consider the sedimentological context: changes in sedimentation regime can produce variations in sulfur isotopic signals as large as those caused by shifts in the ocean chemistry (Fike et al., 2015). For example, ~75‰ variations in $\delta^{34}S_{py}$ associated with glacial-interglacial changes in the sedimentation rate (Pasquier et al., 2017) are comparable in magnitude to the $\delta^{34}S_{py}$ excursions found during the Cambrian Steptoean Positive Carbon Isotope Excursion (SPICE) event, and those excursions have been interpreted to reflect enhanced pyrite burial and changes in the ocean chemistry (Gill et al., 2011). Moreover, ^{34}S-enriched pyrites, which have been linked to low seawater sulfate concentrations during the late Proterozoic (< 2 mM; Ries et al., 2009), have also been observed in modern marine sediments with a high sulfate concentration (~28 mM; Jørgensen et al., 2004; Aller et al., 2010).

The East China Sea (ECS) is characterized by a high influx of terrigenous materials from surrounding rivers, including one of largest rivers in the world, the Changjiang River (Yang et al., 2014). On the inner shelf of the ECS, where abundant organic carbon and authigenic pyrite are buried (Yao et al., 2015; Zhu et al., 2016), mud depocenters are well developed. Previous studies on the diagenetic processes of sedimentary pyrite in the ECS have documented that the rate of MSR is limited by the low availability of organic carbon (Lin et al., 2000), which, in combination with sulfur disproportionation, has been proposed to account for the enrichment of ^{32}S in sedimentary pyrite in the ECS (Zhu et al., 2016). These limited studies have focused only on surficial or near-surface (i.e., short cores) sediments, and thus, any potential coupling of sulfur biogeochemical cycling with the changing sedimentation regime over geologic time has not yet been examined. Therefore, new data are needed to provide insight into the sedimentary and diagenetic processes of pyrite and fluctuating redox conditions in the mud depocenter coupled with the sedimentation regime since the late Pleistocene. To address this gap, a long sedimentary core penetrating the sediment column of the mud depocenter was drilled in the ECS. Here, we employ a multiproxy approach to study sedimentary pyrite with a focus on its sulfur abundance and isotopic composition associated with the total carbon and carbonate contents of bulk sediments. This study demonstrates that the sedimentation rate plays a critical role in determining the pyrite sulfur isotopic composition in a shallow depositional environment.

2. Regional setting

The ECS, with total area of $7.7 \times 10^5\,km^2$, is one of the largest marginal seas in the world (Fig. 1) and receives an enormous influx of terrigenous materials from surrounding rivers, such as the Changjiang River, local rivers from Zhejiang and Fujian Provinces, and mountainous rivers from Taiwan (Xu et al., 2012; Liu et al., 2018b). The Changjiang River, originating on the Tibetan Plateau at an elevation of 6600 m, is the greatest supplier of terrigenous materials to the ECS, including $2–5 \times 10^6\,t\,yr^{-1}$ of terrestrial organic carbon (Bianchi and Allison, 2009), $8.96 \times 10^{11}\,km^3\,yr^{-1}$ of freshwater and $3.90 \times 10^8\,t\,yr^{-1}$ of sediment (Yang et al., 2015). Fine-grained sediments discharged by the Changjiang River tend to be deposited along the south bank of the river mouth during the summer and are then resuspended to be delivered southward along the inner shelf of the ECS by the Zhejiang-Fujian Coastal Current (ZFCC; Fig. 1) during the East Asian winter monsoon (EAWM). The Zhejiang-Fujian mud depocenter is regulated by the northward Taiwan Warm Current (TWC) and by the southward ZFCC (Liu et al., 2006). Due to a dynamic barrier caused by the interaction of these current systems and offshore upwelling, substantial amounts of these sediments are trapped on the inner shelf (Liu et al., 2018a), forming a northern mud depocenter off the Changjiang Estuary and another southern occurrence along the Zhejiang-Fujian coast (Fig. 1). The sediments from both mud depocenters are enriched in organic matter, which is derived from both terrigenous and marine organic carbon (Yao et al., 2015).

Based on seismic profiles, the mud belt deposited on the inner shelf spans from the Changjiang River mouth southwards ~800 km to the southwestern corner of the Taiwan Strait (Liu et al., 2006). This fine-grained muddy deposit is 40 m thick (i.e., Units III and IV in Fig. 1) between the 20- and 30-m isobaths with a width of 100 km (Xu et al., 2012). The southern depocenter has been fed by sediments derived from the Changjiang River since ~11 ka (Xu et al., 2011) and has been well developed during the sea-level highstand since ~7 ka (Li et al., 2014), when the modern current system was established. The sedimentation regime on the inner shelf of the ECS is related to sea-level fluctuations and climatic conditions in addition to the current system, which in turn influences the biogeochemical cycling of C-S-Fe in this area.

3. Materials and methods

3.1. Core EC2005

Core EC2005 was drilled at a depth of 60.2 m below the seafloor (mbsf) during a research cruise with the research vessel *Kan 407* at a water depth of 36 m on the southern mud depocenter of the East China Sea (121°20.0036′E, 27°25.0036′N; Fig. 1) in November 2005. According to 16 accelerator mass spectrometry (AMS)-^{14}C ages calculated by CALIB 5.0.1 (Fig. 1), the core sediments cover the last 16.5 ka (Xu et al., 2009).

3.2. Carbonate and total organic carbon (TOC) analysis

The bulk sediments were dried and ground to homogeneous powders of 200 mesh size particles to establish the total carbon (TC) contents. An additional 0.1 g of powder for each sample was dissolved with 1 mol/l HCl in 40% for 48 h and then rinsed four times with deionized water to remove carbonates for TOC measurements. The total inorganic carbon (TIC) contents were calculated by subtracting the TOC contents from the TC contents. To express the TIC content as percent calcium carbonate ($CaCO_3$), the content of $CaCO_3$ was calculated by $CaCO_3$ (%) = TIC * 8.33. The measurements were performed on a Thermal EA 1112 CHN elemental analyser with an analytical precision of 0.1% at the Institute of Oceanology, Chinese Academy of Sciences (IOCAS).

3.3. Pyrite extraction and isotopic measurement

Pyrite was extracted from the bulk sediments as chromium-reducible sulfur (CRS) according to the method described by Canfield et al. (1986). Samples were heated to 186 °C (± 10 °C) under constant stirring for 4 h with 6 M HCl and 2 M chromium (II) chloride solution while being continually flushed with N_2 gas. The evolved gas was passed through a water trap before bubbling into a test tube containing silver nitrate solution in deionized H_2O. Precipitated silver sulfide was then rinsed and dried overnight; the reproducibility was under 5% for repeated analyses. The bulk sediment pyrite abundance (wt% pyrite)

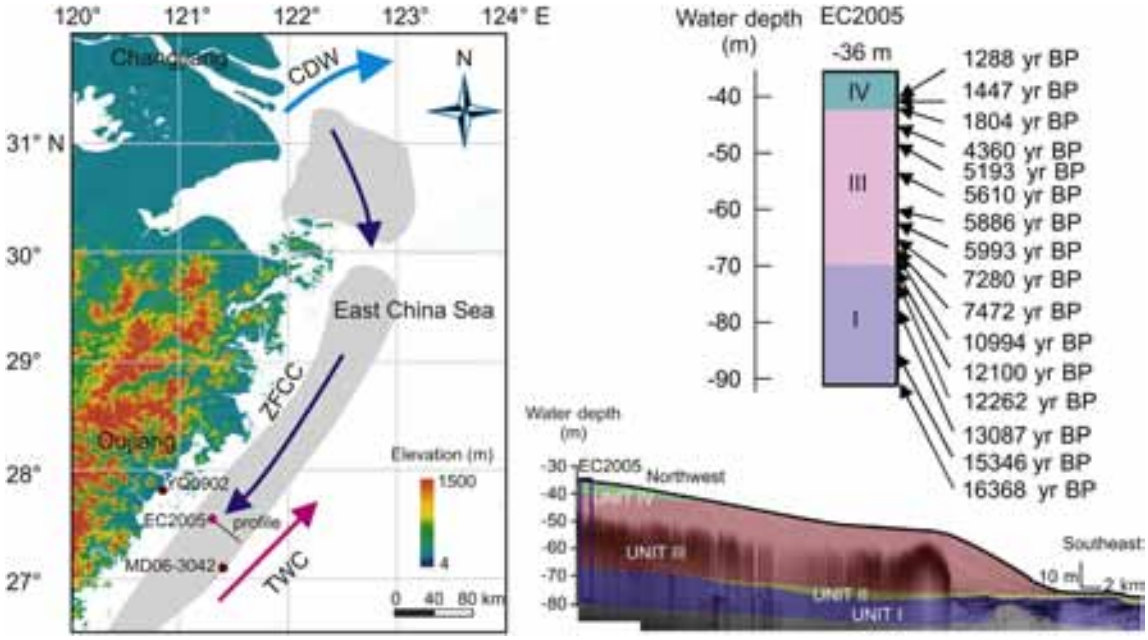

Fig. 1. Study area and the location of core EC2005. The mud belt is represented by the shaded zone. Currents include the Changjiang Diluted Water (CDW), the Zhejiang-Fujian Coastal Current (ZFCC), and the Taiwan Warm Current (TWC). The seismic profile is modified from Xu et al. (2012); Units I (late Pleistocene sandy sediments), II (sediments deposited during sea-level transgression between 14 and 11 ka), III (muddy sediments deposited between 11 and 2 ka) and IV (recent muddy sediments with intensive human activities after 2 ka) are indicated by blue, yellow, red and green, respectively. The age dates of core EC2005 are from Xu et al. (2009). The locations of core MD06-3042 (Liu et al., 2017) and core YQ0902 (Shang et al., 2018) are also presented. (For interpretation of the references to color in this figure legend, the reader is referred to the web version of this article.)

was calculated from the CRS precipitate yield relative to the initial mass used for the extraction.

Approximately 350 μg of sulfide was analysed using a Costech ECS 4010 elemental analyser coupled to a Thermo Finnigan Delta V Plus mass spectrometer at Washington University in St. Louis. The sulfur isotope value of the sample is expressed in standard delta notation as per mil (‰) deviations from the Vienna Canyon Diablo Troilite (V-CDT). Isotopic measurements were calibrated against international standards IAEA-S-1 ($\delta^{34}S = -0.3‰$), IAEA-S-3 ($\delta^{34}S = -32.55‰$) and NBS-127 ($\delta^{34}S = +21.1‰$) with analytical errors of < 0.3‰ (1σ) for $\delta^{34}S$.

3.4. Pyrite identification

Pyrite crystals were identified and handpicked from the coarse fraction (grain size ≥ 65 μm) under a microscope. The morphology and geochemistry of sedimentary pyrite were examined using a Hitachi S-3400 N scanning electron microscope (SEM) in energy dispersive spectrum (EDS) mode at IOCAS.

3.5. Statistical analysis

To examine the correlations between the measured parameters and to test whether those correlations are statistically significant, a Pearson correlation analysis with a two-tailed test was performed using SPSS 21.

4. Results

4.1. Sediment composition

According to a previous study (Xu et al., 2011), the core sediments show a general upward fining trend, transitioning from sandy silt to clayey silt from the base to the top (Fig. 2a), with two abrupt decreases in the sand fraction at 50.85 and 36.77 mbsf corresponding to 15.35 and 12.26 ka, respectively, in the age-depth curve (Fig. 2b). Sediments above 28.05 mbsf (7.28 ka) are composed purely of clayey silt, representing the deposits of the mud depocenter (Fig. 2a). All the core sediments are predominantly terrestrial, as reflected by their low carbonate contents (ranging from 1.95 to 14.83 wt% with an average of 5.92 wt%; Fig. 2c). The TOC contents are low throughout the core, ranging from 0.11 to 0.83 wt% with an average value of 0.62 wt% (Fig. 2d) and showing a slightly increasing trend in shallower samples. The lower part (below 28.05 mbsf) of the core sediments is characterized by sharp fluctuations in the TOC contents, while the upper core sediments show relatively constant values (Fig. 2d).

4.2. Pyrite sulfur contents and sulfur isotopic compositions

The total pyrite sulfur contents (TS_{py}) range from 0 to 0.98 wt% with an average of 0.35 wt% (Fig. 2e). TS_{py} shows its lowest value at the core bottom (< 0.10 wt%), followed by a rapid increase at 36.77 mbsf (arrow in Fig. 2e). The TS_{py} contents maintain high values between 36.77 and 8.97 mbsf with an average of 0.61 wt%, which is followed by a zone of low TS_{py} values within the top 8.97 m.

Our results show that the $\delta^{34}S_{py}$ values of pyrite range from −38.2 to 15.0‰ with an average of −14.6‰, encompassing a range of 53.2‰ (Fig. 2f). In the coarse-grained sediments at the base of the core, the $\delta^{34}S_{py}$ values are generally between −10 and 10‰. The transition to fine-grained sediments is marked by increased variability in the $\delta^{34}S_{py}$ values. Four intervals of low $\delta^{34}S$ values (< ~ − 30‰) are recorded, with the lowest $\delta^{34}S_{py}$ values observed in the uppermost interval above 12.33 mbsf (average of −33.9‰). Three intervals of elevated $\delta^{34}S_{py}$ values (with values up to +15‰) are interposed between them (at 36.5 mbsf, 29.5 mbsf, and 20.6 mbsf). The transitions between the depleted and enriched intervals are generally characterized by abrupt changes in $\delta^{34}S_{py}$, although the upper transition is more gradual (arrow in Fig. 2f).

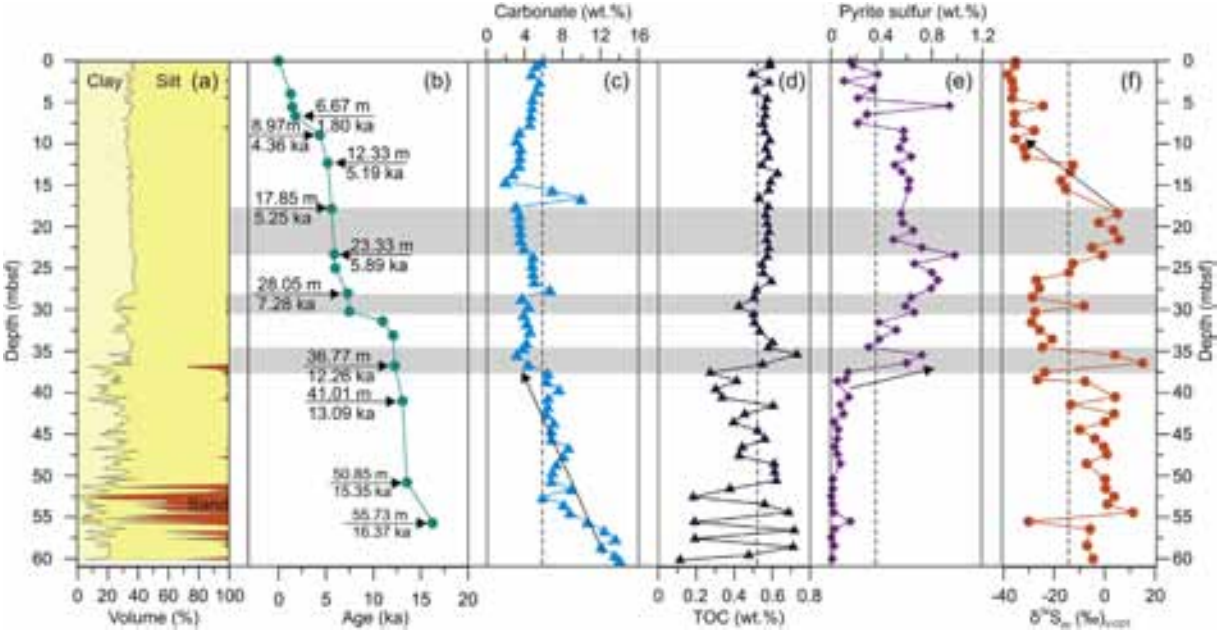

Fig. 2. Sediment composition and pyrite sulfur abundance and isotopic composition of core EC2005. (a–b) Grain size composition and age model of core EC2005 based on Xu et al. (2009); (c–d) carbonate and total organic carbon (TOC) contents in the bulk sediments of core EC2005; (e–f) total pyrite sulfur contents and isotopic composition of core EC2005. Dashed lines represent the corresponding average values in panels c–f. Shaded regions indicate intervals of elevated pyrite contents and high $\delta^{34}S_{py}$ values.

4.3. Morphology of sedimentary pyrite

Most of the handpicked pyrites from core sediments are aggregations of hundreds to thousands of individual framboids (Fig. 3), which are observed only in the upper section above 41 m. The most common morphological types of pyrite aggregates observed under SEM are as follows: (1) organism-filling aggregates, e.g., in the chambers of foraminiferal tests (Fig. 3a); (2) spherical shapes with a range of diameters (Fig. 3d); (3) rod-like shapes with variations in both the diameter and the length (Fig. 3e); and (4) irregular aggregates, the most common morphological form (Fig. 3f). In detail, individual framboids usually consist of octahedral and irregular pyrite microcrystals without overgrowth on the framboids (Fig. 3b–c).

The SEM-EDS analysis extends below the surface of pyrites that show variable shapes (Fig. 3g–i). EDS spectra of pyrite show two distinctive, narrow iron and sulfur peaks, which is typical for iron sulfide minerals. The EDS mode on the Hitachi S-3400 N SEM may have experienced elemental interference from the surrounding matrix or other minerals during the analysis of pyrites; thus, other elements, such as oxygen (O), calcium (Ca), and silicon (Si), could have been captured in the EDS spectra (Fig. 3g–i).

5. Discussion

5.1. Sedimentation regime since the late Pleistocene

The depositional environments on the ECS shelf were controlled by sea-level fluctuations during the late Pleistocene and the Holocene (Li et al., 2014), which would have influenced the geochemical signals of shelf sediments (Fig. 4). In marine sediments, ratios of the TOC content to TS_{py} have been widely used to indicate the depositional environment, with an average of ~2.8 for normal shelf environments (Berner and Raiswell, 1984). According to the relative sea-level curve derived from the mud sediments on the ECS (Dong et al., 2018), the lower core sediments were deposited in a freshwater environment (Fig. 4a), which is also reflected by the high TOC/TS_{py} ratios (up to 61.5; Fig. 4b), indicating a limited influence of seawater in the core location before 12.26 ka. The TOC/TS_{py} ratios also present a general decreasing trend until they fall within the scope of a marine environment at approximately 36.77 m (arrow in Fig. 4b), which is in accordance with the sea-level rise during the last deglaciation (Fig. 4f). The global sea-level rise during the last deglaciation was punctuated by a period of lower rates during the Younger Dryas (YD; 12.5–11.5 ka; Lambeck et al., 2014), which corresponds to a tidal flat environment in the study area (Fig. 4a; Dong et al., 2018). After the YD, the sea-level rates accelerated again and reached their highstand at approximately 7.28 ka (Fig. 4g), which is associated with the initial development of the mud depocenter on the inner shelf of the ECS as indicated by constant mean grain size values (Fig. 4e).

In spite of the relatively stable depositional environment during the sea-level highstand, the sedimentation rates at the core location show significant fluctuations (Fig. 4d). In particular, an interval with an extremely high sedimentation rate is present between 23.33 and 17.85 mbsf with an average of ~2 cm/yr during 5.89–5.25 ka. This interval with a high sedimentation rate has been interpreted to be the result of the enhanced ZFCC in response to a stronger EAWM (Xu et al., 2009) because most terrigenous sediments in the mud depocenter are mainly derived from the Changjiang River and are transported southwards by coastal currents in winter (Liu et al., 2006; Liu et al., 2018a). This interval with a high sedimentation rate has also been confirmed by another sedimentary record from core YQ0902 (Shang et al., 2018; see its location in Fig. 1). Another interval with such a high sedimentation rate (up to 2.3 cm/yr) is observed between 36.77 and 33.09 mbsf during 12.26–12.10 ka, which is also recorded by other core sediments on the inner shelf of the ECS (e.g., core MD06-3042 in Fig. 1; Liu et al., 2017), corresponding to a strong EAWM during the YD cooling interval. Therefore, the sedimentation regime in the study area was constrained by changes in the global sea level and inland climate (i.e., the EAWM) since 16.5 ka, which in turn could modulate sulfur cycling in these mud-rich sediments.

5.2. Factors controlling the pyrite sulfur abundance

In sediments, organic matter decomposition driven by MSR leads to

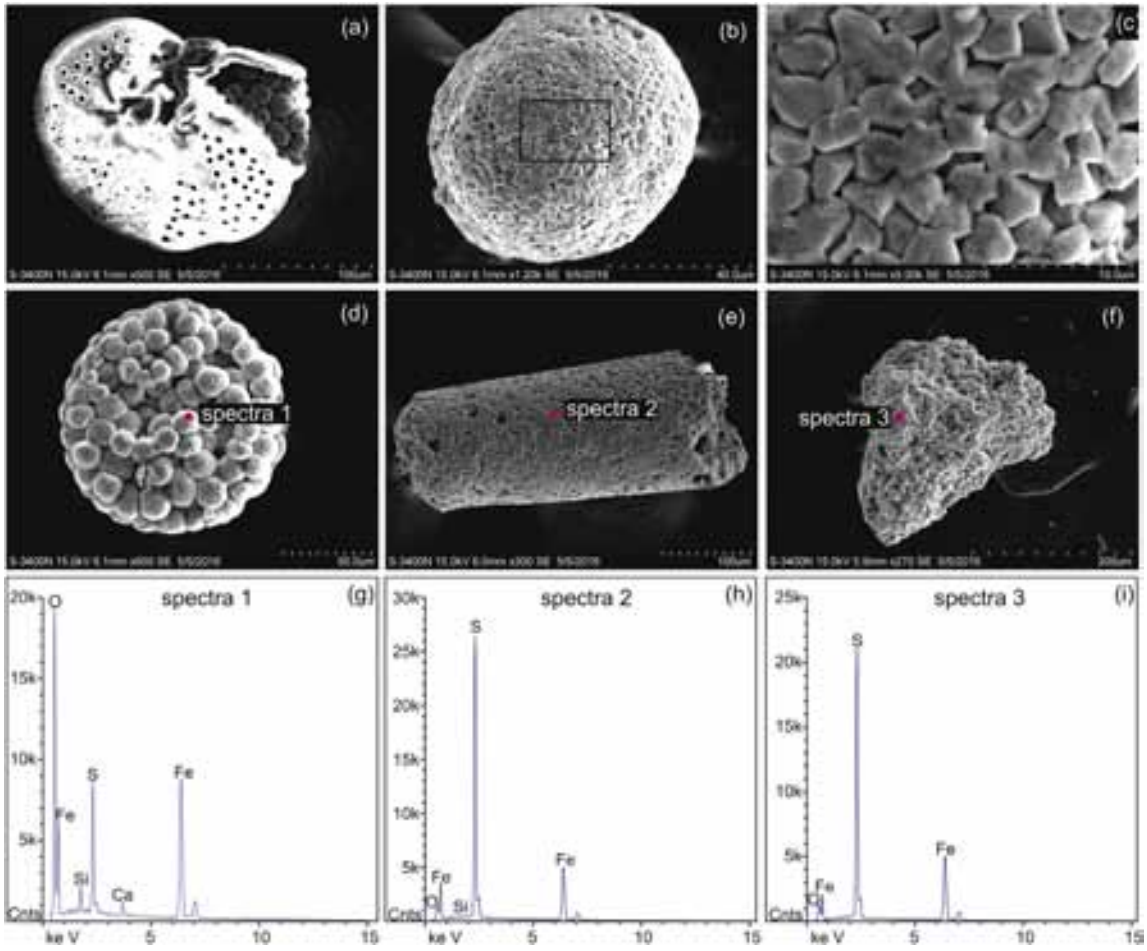

Fig. 3. Representative scanning electron microscope (SEM) images and energy dispersive spectrum (EDS) graphs of pyrite in core sediments. (a) Aggregates filled in a foraminiferal chamber; (b) pyrite framboids formed by octahedral microcrystals; (c) enlarged view of (b); (d) spherical pyrite aggregates (the pyrites in panels a–d are from sediments at 5.48–5.50 mbsf); (e–f) rod-like and irregular massive pyrite aggregates at 32.48–32.50 mbsf; (g–i) EDS graphs of sedimentary pyrite in panels d–f, where pink solid circles show the EDS analysis spot on the pyrite. (For interpretation of the references to color in this figure legend, the reader is referred to the web version of this article.)

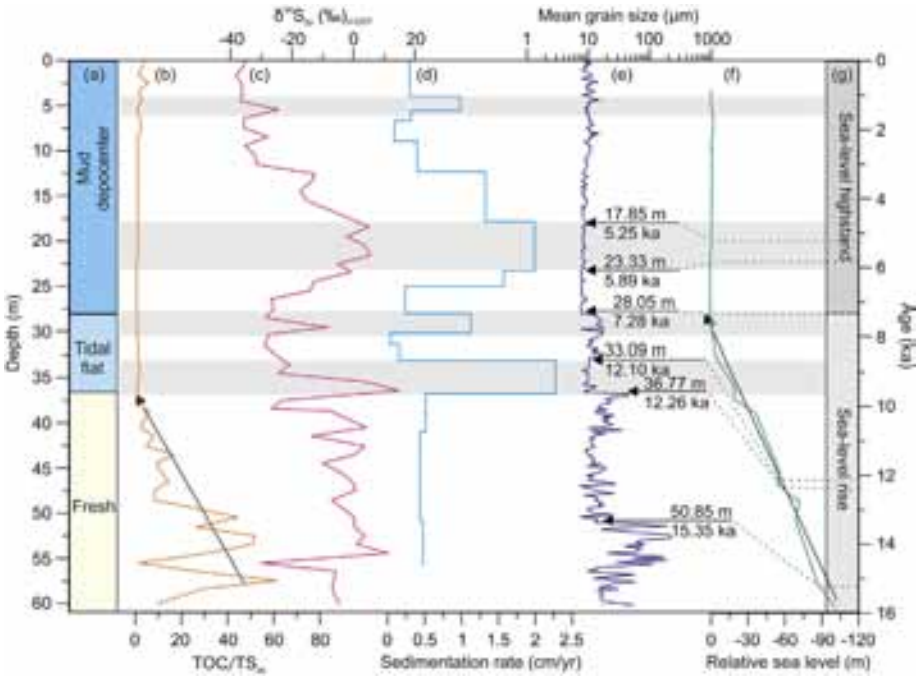

Fig. 4. Variation in pyrite sulfur isotopic compositions related to shifts in the sedimentation regime of core EC2005. (a) Depositional environments according to Xu et al. (2009); (b) ratios of the total organic carbon content to the total sulfur (TOC/TS_{sy}); (c) pyrite sulfur isotopic compositions; (d–e) sedimentation rates (cm/yr) and mean grain sizes (μm) based on Xu et al. (2009); (f–g) sea-level reconstruction off East China; data from Lambeck et al. (2014).

the production of H_2S (Berner, 1984), where microorganisms couple the reduction of sulfate (SO_4^{2-}) to hydrogen sulfide (H_2S) with the oxidation of organic materials (represented by CH_2O) to bicarbonate (HCO_3^-), which is expressed in Eq. (1).

$$SO_4^{2-} + 2CH_2O \rightarrow H_2S + 2HCO_3^- \quad (1)$$

A portion of the H_2S that is produced may react with reactive iron to form iron sulfide minerals, such as pyrite, which can be buried and preserved over geologic time (Berner, 1984). Accordingly, the pyrite contents in sediments mainly depend on the following factors: (i) the reactivity and quantity of organic matter; (ii) the rates of supply of dissolved sulfate; (iii) the amount and reactivity of iron; (iv) the redox conditions and rates of sedimentation (e.g., Jørgensen, 1977, 1982, 1990; Berner, 1984; Raiswell et al., 1988); and (v) the anaerobic oxidation of methane (AOM) in methane-rich sediment (e.g., Jørgensen et al., 2004; Borowski et al., 2013; Lin et al., 2016; Riedinger et al., 2005, 2017). In freshwater sediments, the pyrite contents are generally limited by low sulfate concentrations (Berner, 1984), and thus, pyrite sulfur contents are very low in the lower (freshwater) section of EC2005, when the sea level had not yet reached the core location (Fig. 5a).

When the study area was under the influence of seawater, organic matter may have been the major control on pyrite formation because sulfate and iron are abundant in the mud-rich sediments of the ECS (Huang and Lin, 1995). Previous studies on the ECS continental shelf sediments demonstrated that organic carbon is the primary factor controlling the pyrite burial rates (Lin et al., 2000), suggesting that sulfate reduction might be suppressed due to the limited availability of labile organic matter in the inner shelf sediments of the ECS (Zhu et al., 2016). However, our results show only a moderate positive correlation between the pyrite sulfur and TOC contents ($r = 0.36$, $p < 0.01$; Fig. 5a), indicating that the TOC content is not the main limiting factor controlling the pyrite sulfur contents in the study area. Another process possibly related to the formation of pyrite is the AOM at the sulfate-methane transition zone (SMTZ), which is independent of the quantity and quality of the TOC (e.g., Jørgensen et al., 2004; Riedinger et al., 2017). Though our previous work on authigenic gypsum and pyrite implied that the AOM might be involved in the formation of pyrite in the uppermost section (4–0 mbsf) of this core (Liu et al., 2018c), it is difficult to calculate the impact of the AOM in the SMTZ on pyrite formation without porewater data. Rapid sedimentation rates can enhance the preservation of labile organic matter by reducing the time organic matter spends in the zone of aerobic respiration (Canfield, 1991). However, very high sedimentation rates would dilute the amount of organic matter and could lead to an advective system with regard to sulfate in the porewater that outpaces diffusion and strongly impacts microbial activity in the sediment (Riedinger et al., 2005). Our TOC contents show only a weak positive correlation with sedimentation rates ($r = 0.26$, $p < 0.05$; Fig. 5b), indicating that a rapid sedimentation rate might not enhance the burial efficiency of organic matter. Another possible explanation for the weak relationship between the TOC content and sedimentation rate is that the TOC represents the organic matter remaining after diagenesis. In fact, the TOC contents show a significantly negative correlation with the grain size ($r = 0.59$, $p < 0.01$; Fig. 5c), indicating that fine-grained sediments favour the preservation of organic matter. MSR is also impacted by different types of organic matter, that is, different types of electron donors (Sim et al., 2011b). Thus, despite negligible changes in the TOC content associated with changes in the sedimentation rate, the TOC content may impact the microbial sulfur cycle.

5.3. Sulfur isotopic fractionation since the late Pleistocene

MSR is the primary pathway that constrains the extent of sulfur isotopic fractionation between produced sulfide and the initial sulfate (Canfield, 2001a) expressed as $\Delta^{34}S = \delta^{34}S_{sulfate} - \delta^{34}S_{sulfide}$. Because the sulfur isotopic fractionation between dissolved sulfide and precipitating sulfide minerals associated with pyrite formation is low (< 1‰) (Price and Shieh, 1979), the sulfur isotopic composition of dissolved sulfide is assumed to be captured within pyrite in this study.

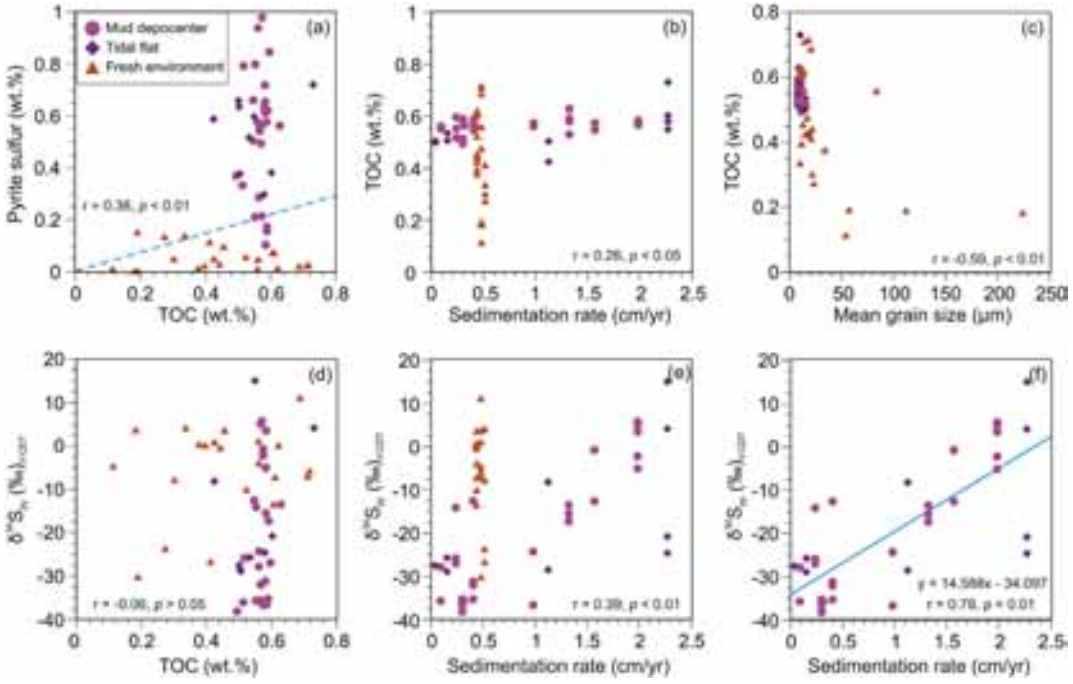

Fig. 5. Controlling factors for the abundance and isotopic composition of pyrite sulfur in core EC2005. (a) Pyrite sulfur content plotted as a function of the total organic carbon (TOC) content. Dashed line represents the TOC/TS_{py} weight ratio of 2.8 for normal marine shelf sediments (Berner and Raiswell, 1984). (b–c) TOC contents plotted against (b) the sedimentation rate and (c) the mean grain size value. (d) Relationship between the pyrite sulfur isotopic composition and TOC content. (e–f) Pyrite sulfur isotopic compositions constrained by the sedimentation rate in (e) all the environments and (f) the marine environment. Statistical analyses of the correlations between measured parameters were performed by SPSS 21.

In freshwater environments, where sulfate concentrations are typically low, ambient sulfate is often (nearly) completely consumed during MSR, resulting in ^{34}S-enriched sulfide that approaches the initial composition of ambient sulfate (Gomes and Hurtgen, 2015). Consequently, the resulting pyrite produced becomes enriched in ^{34}S, resulting in a low Δ^{34}S value. Thus, the $\delta^{34}S_{py}$ values from the freshwater environments of EC2005 mostly approximate the range of the freshwater sulfate between −5 and 15‰ (Nehlich, 2015), which is similar to the sulfur isotope distribution in the lake sediments of the Black Sea during the late Pleistocene (Calvert et al., 1996). The only more negative $\delta^{34}S_{py}$ value of approximately 55.5 mbsf indicates that sulfur isotopic fractionation should occur even when the sulfate concentration is low (i.e., Gomes and Hurtgen, 2015). It is important to note that this low Δ^{34}S value reflects the restricted-system consumption of sulfate and therefore should not be used to infer small biological fractionation during MSR (Gomes and Hurtgen, 2013).

In marine environments that are not limited by the availability of sulfate, sulfur isotopic fractionation via MSR can reach 70‰ (Canfield et al., 2010; Sim et al., 2011a). In our $\delta^{34}S_{py}$ profile, all the large depletions in ^{34}S are associated with slow sedimentation rates (Fig. 4c–d), which could be related to the following two possible mechanisms. Due to the slow sedimentation rate, the organic matter supply will be reduced, and the organic matter will spend more time in the zone of aerobic respiration; thus, the MSR rate will remain low, leading to significant sulfur isotopic fractionation (Goldhaber and Kaplan, 1975; Sim et al., 2011b; Leavitt et al., 2013; Wing and Halevy, 2014). However, the TOC content is quite constant in the study core and is not controlled by the sedimentation rate (Fig. 5b), suggesting that the TOC content is unlikely to lead to variable biological fractionation during MSR, which is supported by the weak correlation between the $\delta^{34}S_{py}$ and TOC values ($r = -0.06$, $p > 0.05$; Fig. 5d).

Alternatively, slow sedimentation rates could promote diffusive exchange between porewater and seawater sulfate, forming an “open” diagenetic system (McKay and Longstaffe, 2003), where a constant seawater sulfate supply precludes ^{34}S enrichment in porewater sulfate and therefore in the resulting sulfide (Claypool, 2004; Gomes and Hurtgen, 2015). Assuming a modern seawater $\delta^{34}S_{sulfate}$ value of 21.2‰ (Tostevin et al., 2014), pyrite sulfur has significant isotopic fractionations above 12.33 mbsf in core EC2005 with average Δ^{34}S values reaching as high as 55.1‰. Such extensive sulfur isotopic fractionation between seawater sulfate and sulfide ($\Delta^{34}S > 46$‰) has been attributed to the disproportionation of intermediate sulfur species in addition to MSR (Jørgensen, 1990; Canfield and Thamdrup, 1994). Considering the presence of S^0 in mud sediments on the ECS inner shelf (Zhu et al., 2016) and the unsteady dynamic conditions therein, the large isotopic fractionation may involve the disproportionation of S^0 (or other intermediate oxidized S species) (Passier et al., 1997; Habicht and Canfield, 2001; Böttcher et al., 2001). However, the significant depletion of ^{34}S and large fractionations observed herein are within the range that could be explained solely by MSR (Wortmann et al., 2001; Sim et al., 2011a; Brunner and Bernasconi, 2005). Therefore, the highly ^{34}S-depleted pyrites observed during slow sedimentation rates are most likely to be explained by MSR in an open diagenetic system and may be accompanied by microbial disproportionation.

In comparison, pyrites between 23.33 and 17.85 mbsf are characterized by the highest δ^{34}S values, representing low Δ^{34}S values with an average of 20.1‰. Such limited isotopic fractionation has been linked to high sulfate reduction rates (Canfield, 2001a), which could be caused by the more efficient delivery of organic carbon to the reaction zone as a result of rapid sedimentation (Böttcher et al., 2004). Previous studies have documented that a high rate of MSR is likely linked to a rapid sedimentation rate (Claypool, 2004; Pasquier et al., 2017). The TOC content will normally be diluted when the sedimentation rate is very high. However, the TOC content in the sediment has remained constant since 12.3 ka even though the sedimentation rate has varied. This indicates that an enhanced availability of organic matter would be obtained and buried in the sediment during a certain period of high sedimentation rates compared with low sedimentation rates, which may affect the sulfur isotopic fractionation. Therefore, the sulfur isotopic fractionation of MSR could also be affected by the TOC quality or quantity. However, the low TOC contents (average of 0.62 wt%) in our core sediments suggest that it is extremely unlikely that the MSR rates were ever high enough to generate low fractionation during MSR (Fig. 5d). Recent research suggested that MSR could be suppressed by metal reduction due to the high terrigenous inputs of iron oxides in the mud sediments on the ECS inner shelf (Zhao et al., 2018). However, our results suggest that MSR is still one of the most important pathways for organic mineralization in such Fe-rich sediment.

Alternatively, due to rapid sedimentation rates, porewaters can be effectively isolated from the overlying seawaters, and thus, pyrite tends to be produced in a “restricted” diagenetic system (Claypool, 2004; Pasquier et al., 2017; Riedinger et al., 2017). Progressive MSR results in high porewater δ^{34}S values of sulfate and correspondingly enriched δ^{34}S values of H_2S, leading to a parallel increase in the δ^{34}S values of sulfate and sulfide (Gomes and Hurtgen, 2015). A previous study also indicated that relatively rapid burial below the depth where sulfate is added to the sediment via bioturbation and diffusion from the overlying seawater leads to the formation of pyrite with higher δ^{34}S values in the marine environment (McKay and Longstaffe, 2003). The result of this effect is that the $\delta^{34}S_{py}$ values in restricted systems are not as depleted in ^{34}S as those in open systems, and therefore, Δ^{34}S values are low when sedimentation rates are high. Low Δ^{34}S values arising from restricted-system conditions mask the true magnitude of biological fractionation during MSR and therefore should not be used to reconstruct microbial sulfur cycling.

High δ^{34}S values of pyrite sulfur have also been observed in the SMTZ, where sulfate is completely consumed by anaerobic methane oxidation (AMO) and the resulting hydrogen sulfide is enriched in ^{34}S, which leads to the formation of ^{34}S-enriched pyrite (e.g., Jørgensen et al., 2004; Lin et al., 2016; Riedinger et al., 2017). This process was involved in the formation of authigenic gypsum in core EC2005 (Liu et al., 2018c), but it occurred only in limited layers within the uppermost section (4–0 mbsf). Our new pyrite sulfur isotopes between 4 and 0 mbsf are significantly depleted in ^{34}S, suggesting that these pyrite crystals were formed by organoclastic sulfate reduction. In the lower section of core EC2005, the carbonate peak at approximately 17 mbsf might be attributed to authigenic carbonate formation related to AOM and could potentially overprint the pyrite sulfur isotopic signal below this interval. However, in the absence of porewater data, it is impossible to evaluate the influence of AOM on sulfur isotopic fractionation, which requires further investigation of the chemical and isotopic properties of porewater.

5.4. Pyrite sulfur isotopic compositions constrained by the sedimentation rate

The $\delta^{34}S_{py}$ values show a positive relationship with the sedimentation rates ($r = 0.39$, $p < 0.01$; Fig. 5e), indicating a sedimentological constraint on the incorporation of sulfur isotopic signatures into sedimentary pyrites. Such a relationship is more obvious under the marine conditions ($r = 0.78$, $p < 0.01$; Fig. 5f) when the sea level reached the study area. Therefore, we propose a diagenetic model for sulfur isotopic fractionation in core EC2005 (Fig. 6) taking into consideration both the mass balance and the sedimentation rate, where the open-vs.-restricted system behaviour of the porewater as a function of slow-vs.-fast sedimentation is the main factor in the observed diagenetic patterns.

The contents of the reactants involved in pyrite formation (sulfate, organic matter and iron) in seawater are controlled by the climatic conditions in the hinterland and the oceanographic conditions in the ECS (Fig. 6). During the interval of the weakened EAWM, resuspended mud sediments transported south would have declined, leading to

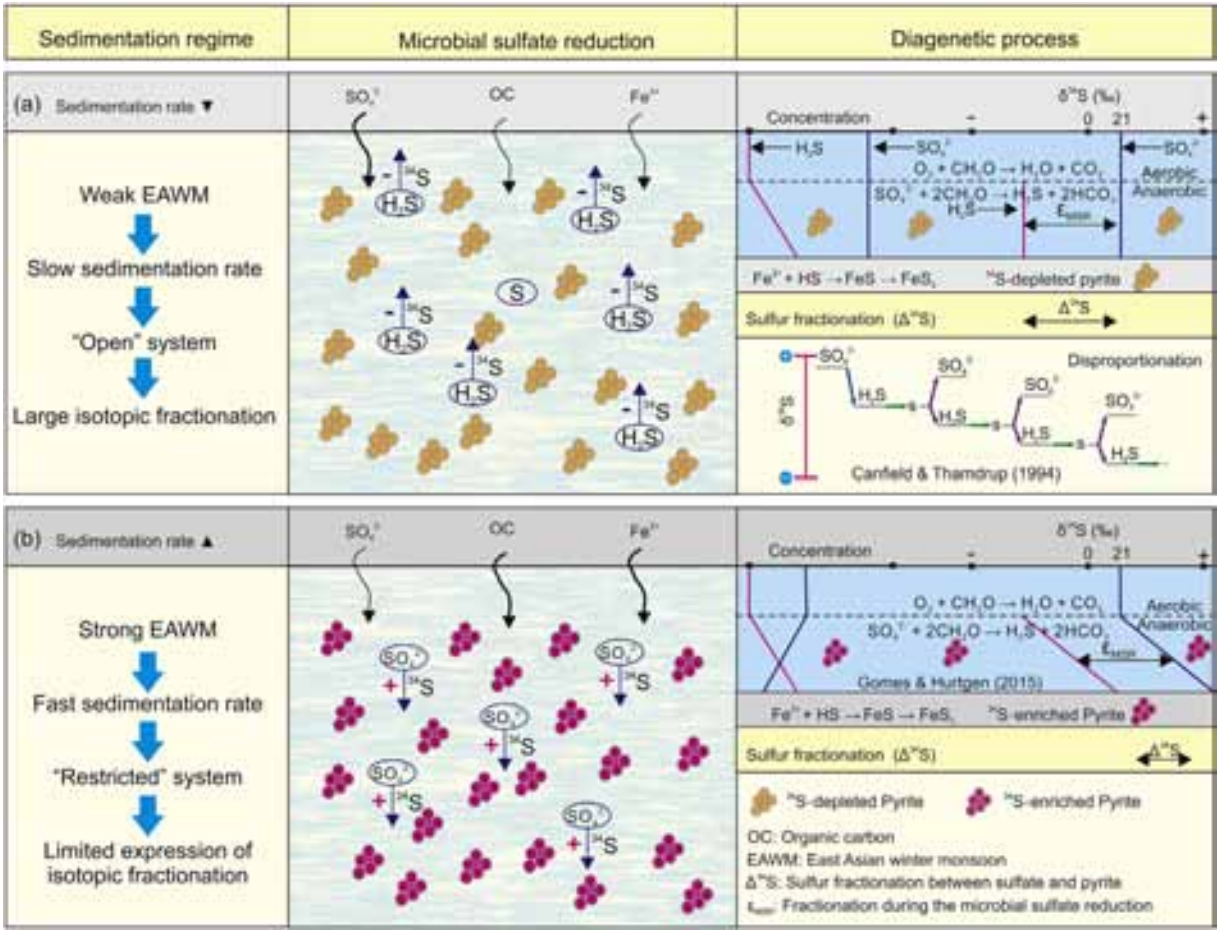

Fig. 6. Diagenetic model of how the sedimentation regime affects the isotopic composition of pyrite on the inner shelf of the East China Sea. (a) Precipitation of substantial ^{34}S-depleted pyrite by microbial sulfate reduction in an "open" diagenetic system. Due to slow sedimentation rates, this process may be combined with sulfur disproportionation, resulting in extensive fractionation ($\Delta^{34}S > 46‰$). (b) Precipitation of limited ^{34}S-depleted pyrite in a "restricted" diagenetic system due to rapid sedimentation rates. The sulfur isotopic composition of porewater sulfate becomes more enriched in ^{34}S in such a system, where the preserved isotopic fractionation between pyrite and sulfate is low, producing limited ^{34}S-depleted pyrites.

slowed sedimentation rates (Fig. 6a). This low sedimentation rate would enhance the communication between porewater and seawater sulfates, forming an open system. In such a digenetic system, the residual sulfate reservoir does not experience substantial drawdown, minimizing any ^{34}S enrichment in porewater sulfate with continued MSR. The sulfide produced in such systems therefore remains depleted in ^{34}S (reflecting biological fractionation during MSR), generating pyrite framboids with very low $\delta^{34}S$ values distributed widely throughout the sediment column. In addition, microbial disproportionation might have been involved under these relatively oxidizing conditions (e.g., MnO_2, ferric oxide and S^0; Böttcher et al., 2001; Böttcher and Thamdrup, 2001), possibly contributing to the observed large isotopic fractionation between seawater sulfate and pyrite (high $\Delta^{34}S$) (Fig. 6a).

In contrast, when the EAWM was strong, the sediment rates were high because of enhanced coastal currents (Fig. 6b). Such rapid sedimentation will considerably decrease the connectivity between the porewater sulfate reservoir and the overlying seawater to form a restricted system, where the local porewater sulfate reservoir becomes enriched in ^{34}S as MSR continues. In turn, the produced sulfide becomes enriched in ^{34}S, which leads to the formation of relatively heavy pyrite following a reaction with available iron, resulting in low $\Delta^{34}S$ values (Fig. 6b) despite the inferred large biological fractionation during MSR.

6. Implications for pyrite sulfur isotopes in geologic time

The isotopic fractionation between coeval sulfate and pyrite from the geological record has been widely used to reconstruct the seawater chemistry and redox conditions in geologic time (Jones and Fike, 2013; Algeo et al., 2015). However, recent studies have demonstrated that local depositional environments have significant impacts on the sulfur abundance and isotopic composition of both sulfate and sulfide, especially in shallow water environments (Fike et al., 2015 and references therein). For example, unsteady depositional conditions from tropical mobile Amazon mud belts result in the formation of pyrites with unusually high $\delta^{34}S$ values ranging from 0‰ to > 30‰ due to physical reworking (Aller et al., 2010). Similarly, sedimentary pyrite from the shelf of the Gulf of Lion preserves striking sulfur isotopic fluctuations corresponding to glacial-interglacial changes in the depositional environment rather than to changes in seawater chemistry (Pasquier et al., 2017). Another widely referred case study is the enrichment of $\delta^{34}S$ in pyrite related to the global mass extinction at the end of the late Ordovician (Hammarlund et al., 2012; Jones and Fike, 2013); however, this positive excursion in $\delta^{34}S$py could also have been modulated by local sedimentary factors, especially in the proximal area (e.g., Jones and Fike, 2013; Ahm et al., 2017).

Our observations of substantial sulfur isotopic fluctuations in pyrites from the sediments on the ECS inner shelf suggest that these values were modulated by the ambient sedimentation regime, specifically as the result of sedimentation rates regulating the diffusive exchange

between porewater and the overlying seawater. Therefore, we suggest that when using sulfur isotopic compositions to reconstruct marine sulfur cycling over geologic time, it is essential to couple the resulting isotopic data with observations of their depositional environment, especially for shallow sedimentary environments with physical reworking and for facies characterized by variable sedimentation rates.

7. Conclusions

Our results from the mud belt on the inner shelf of the ECS allow us to make a comprehensive evaluation of the complex interactions between the sedimentary processes and hydrodynamics involved in the sulfur isotopic composition of pyrite since the late Pleistocene. On the basis of multiple proxies, we conclude that local depositional conditions controlled the abundance and sulfur isotopic composition of pyrite recorded in core EC2005.

(1) During freshwater conditions prior to the late Pleistocene deglacial sea-level rise, the sediments were characterized by a low abundance of pyrite sulfur with limited isotopic fractionation due to low sulfate concentrations.

(2) In contrast, during marine deposition caused by deglacial sea-level rise, the pyrite sulfur isotopic compositions were more variable and appear to have been modulated mainly by the sedimentation rate. Slow sedimentation could promote the communication between porewater and underlying seawater, forming an “open” diagenetic system that could enable large biological sulfur isotopic fractionations during MSR to be preserved in the sedimentary pyrite record; in comparison, a rapid sedimentation rate would lead to a “restricted” system, where the expression of the isotopic fractionation during MSR would be limited by closed-system distillation.

(3) We finally propose a diagenetic model to explain the changes in the sulfur isotopic composition as a function of the sedimentation rate, which modulates the connectivity between porewater and seawater and results in a shift in diagenetic systems (open vs. restricted).

These new findings indicate that large fluctuations in the sulfur isotopic compositions of pyrite could be caused by local changes in the depositional environment without the need to invoke any changes in the ocean chemistry. Therefore, we provide new insights on how the sedimentation regime regulates sulfur diagenesis in marginal sediments and suggest that understanding the depositional environment where pyrites formed is critical when using their sulfur isotopic records to reconstruct paleoenvironmental conditions in geologic time.

Acknowledgements

We thank the crew of *Kan 407* for collecting the cores used in this study. Editor-in-chief Michael Böttcher and two anonymous reviewers are thanked for their constructive comments and reviews that greatly improved an earlier version of this manuscript. This work was supported by the National Natural Science Foundation of China (41430965; 41606062), the Senior User Project of RV *KEXUE* (KEXUE2017G1), and the State Key Laboratory of Marine Geology, Tongji University (MGK1824).

References

Ahm, A.-S.C., Bjerrum, C.J., Hammarlund, E.U., 2017. Disentangling the record of diagenesis, local redox conditions, and global seawater chemistry during the latest Ordovician glaciation. Earth Planet. Sci. Lett. 459, 145–156.

Algeo, T.J., Luo, G.M., Song, H.Y., Lyons, T.W., Canfield, D.E., 2015. Reconstruction of secular variation in seawater sulfate concentrations. Biogeosciences 12, 2131–2151.

Aller, R.C., Madrid, V., Chistoserdov, A., Aller, J.Y., Heilbrun, C., 2010. Unsteady diagenetic processes and sulfur biogeochemistry in tropical deltaic muds: implications for oceanic isotope cycles and the sedimentary record. Geochim. Cosmochim. Acta 74, 4671–4692.

Berner, R.A., 1984. Sedimentary pyrite formation: an update. Geochim. Cosmochim. Acta 48, 605–615.

Berner, R.A., Raiswell, R., 1984. C/S method for distinguishing freshwater from marine sedimentary rocks. Geology 12, 365–368.

Bianchi, T.S., Allison, M.A., 2009. Large-river delta-front estuaries as natural “recorders” of global environmental change. Proc. Natl. Acad. Sci. U. S. A. 106, 8085–8092.

Borowski, W.S., Rodriguez, N.M., Paull, C.K., Ussler Iii, W., 2013. Are ^{34}S-enriched authigenic sulfide minerals a proxy for elevated methane flux and gas hydrates in the geologic record? Mar. Pet. Geol. 43, 381–395.

Böttcher, M.E., Thamdrup, B., 2001. Anaerobic sulfide oxidation and stable isotope fractionation associated with bacterial sulfur disproportionation in the presence of MnO2. Geochim. Cosmochim. Acta 65, 1573–1581.

Böttcher, M.E., Thamdrup, B., Vennemann, T.W., 2001. Oxygen and sulfur isotope fractionation during anaerobic bacterial disproportionation of elemental sulfur. Geochim. Cosmochim. Acta 65, 1601–1609.

Böttcher, M.E., Khim, B.-K., Suzuki, A., Gehre, M., Wortmann, U.G., Brumsack, H.-J., 2004. Microbial sulfate reduction in deep sediments of the Southwest Pacific (ODP Leg 181, Sites 1119–1125): evidence from stable sulfur isotope fractionation and pore water modeling. Mar. Geol. 205, 249–260.

Brunner, B., Bernasconi, S.M., 2005. A revised isotope fractionation model for dissimilatory sulfate reduction in sulfate reducing bacteria. Geochim. Cosmochim. Acta 69, 4759–4771.

Calvert, S.E., Thode, H.G., Yeung, D., Karlin, R.E., 1996. A stable isotope study of pyrite formation in the Late Pleistocene and Holocene sediments of the Black Sea. Geochim. Cosmochim. Acta 60, 1261–1270.

Canfield, D.E., 1991. Sulfate reduction in deep-sea sediments. Am. J. Sci. 291, 177–188.

Canfield, D., 2001a. Biogeochemistry of sulfur isotopes. Rev. Mineral. Geochem. 43, 607–636.

Canfield, D.E., 2001b. Isotope fractionation by natural populations of sulfate-reducing bacteria. Geochim. Cosmochim. Acta 65, 1117–1124.

Canfield, D.E., Thamdrup, B., 1994. The production of ^{34}S-depleted sulfide during bacterial disproportionation of elemental sulfur. Science 266, 1973–1975.

Canfield, D.E., Raiswell, R., Westrich, J.T., Reaves, C.M., Berner, R.A., 1986. The use of chromium reduction in the analysis of reduced inorganic sulfur in sediments and shales. Chem. Geol. 54, 149–155.

Canfield, D.E., Habicht, K.S., Thamdrup, B., 2000. The Archean sulfur cycle and the early history of atmospheric oxygen. Science 288, 658–661.

Canfield, D.E., Farquhar, J., Zerkle, A.L., 2010. High isotope fractionations during sulfate reduction in a low-sulfate euxinic ocean analog. Geology 38, 415–418.

Claypool, G.E., 2004. Ventilation of marine sediments indicated by depth profiles of pore water sulfate and δ^{34}S. Geochem. Soc. Spec. Publ. 9, 59–65.

Dong, J., Li, A.C., Liu, X.T., Wan, S.M., Feng, X.G., Lu, J., Pei, W.Q., Wang, H.M., 2018. Sea-level oscillations in the East China Sea and their implications for global seawater redistribution during 14.0–10.0 kyr BP. Palaeogeogr. Palaeoclimatol. Palaeoecol. 511, 298–308.

Fike, D.A., Bradley, A.S., Rose, C.V., 2015. Rethinking the ancient sulfur cycle. Annu. Rev. Earth Planet. Sci. 43, 593–622.

Gill, B.C., Lyons, T.W., Young, S.A., Kump, L.R., Knoll, A.H., Saltzman, M.R., 2011. Geochemical evidence for widespread euxinia in the later Cambrian ocean. Nature 469, 80–83.

Goldhaber, M., Kaplan, I., 1975. Controls and consequences of sulfate reduction rates in recent marine sediments. Soil Sci. 119, 42–55.

Gomes, M.L., Hurtgen, M.T., 2013. Sulfur isotope systematics of a euxinic, low-sulfate lake: evaluating the importance of the reservoir effect in modern and ancient oceans. Geology 41, 663–666.

Gomes, M.L., Hurtgen, M.T., 2015. Sulfur isotope fractionation in modern euxinic systems: implications for paleoenvironmental reconstructions of paired sulfate–sulfide isotope records. Geochim. Cosmochim. Acta 157, 39–55.

Habicht, K.S., Canfield, D.E., 2001. Isotope fractionation by sulfate-reducing natural populations and the isotopic composition of sulfide in marine sediments. Geology 29, 555–558.

Hammarlund, E.U., Dahl, T.W., Harper, D.A.T., Bond, D.P.G., Nielsen, A.T., Bjerrum, C.J., Schovsbo, N.H., Schonlaub, H.P., Zalasiewicz, J.A., Canfield, D.E., 2012. A sulfidic driver for the end-Ordovician mass extinction. Earth Planet. Sci. Lett. 331, 128–139.

Huang, K.M., Lin, S.W., 1995. The carbon-sulfide-iron relationship and sulfate reduction rate in the East China Sea continental shelf sediments. Geochem. J. 29, 301–315.

Jones, D.S., Fike, D.A., 2013. Dynamic sulfur and carbon cycling through the end-Ordovician extinction revealed by paired sulfate–pyrite δ^{34}S. Earth Planet. Sci. Lett. 363, 144–155.

Jørgensen, B.B., 1977. The sulfur cycle of a coastal marine sediment (Limfjorden, Denmark). Limnol. Oceanogr. 22, 814–832.

Jørgensen, B.B., 1982. Mineralization of organic matter in the sea bed—the role of sulphate reduction. Nature 296, 643–645.

Jørgensen, B.B., 1990. A thiosulfate shunt in the sulfur cycle of marine sediments. Science 249, 152–154.

Jørgensen, B.B., Böttcher, M.E., Lüschen, H., Neretin, L.N., Volkov, I.I., 2004. Anaerobic methane oxidation and a deep H_2S sink generate isotopically heavy sulfides in Black Sea sediments. Geochim. Cosmochim. Acta 68, 2095–2118.

Kaplan, I.R., Rittenberg, S.C., 1964. Microbiological fractionation of sulphur isotopes. J. Gen. Microbiol. 34 (2), 195–212.

Kunzmann, M., Bui, T.H., Crockford, P.W., Halverson, G.P., Scott, C., Lyons, T.W., Wing, B.A., 2017. Bacterial sulfur disproportionation constrains timing of Neoproterozoic oxygenation. Geology 45, 207–210.

Lambeck, K., Rouby, H., Purcell, A., Sun, Y., Sambridge, M., 2014. Sea level and global ice volumes from the Last Glacial Maximum to the Holocene. Proc. Natl. Acad. Sci. U. S. A. 111, 15296–15303.

Leavitt, W.D., Halevy, I., Bradley, A.S., Johnston, D.T., 2013. Influence of sulfate reduction rates on the Phanerozoic sulfur isotope record. Proc. Natl. Acad. Sci. U. S. A. 110, 11244–11249.

Li, G.X., Li, P., Liu, Y., Qiao, L.L., Ma, Y.Y., Xu, J.S., Yang, Z.G., 2014. Sedimentary system response to the global sea level change in the East China Seas since the last glacial maximum. Earth-Sci. Rev. 139, 390–405.
Lin, S., Huang, K.M., Chen, S.K., 2000. Organic carbon deposition and its control on iron sulfide formation of the southern East China Sea continental shelf sediments. Cont. Shelf Res. 20, 619–635.
Lin, Z.Y., Sun, X.M., Peckmann, J., Lu, Y., Xu, L., Strauss, H., Zhou, H.Y., Gong, J.L., Lu, H.F., Teichert, B.M.A., 2016. How sulfate-driven anaerobic oxidation of methane affects the sulfur isotopic composition of pyrite: a SIMS study from the South China Sea. Chem. Geol. 440, 26–41.
Liu, J.P., Li, A.C., Xu, K.H., Veiozzi, D.M., Yang, Z.S., Milliman, J.D., DeMaster, D., 2006. Sedimentary features of the Yangtze River-derived along-shelf clinoform deposit in the East China Sea. Cont. Shelf Res. 26, 2141–2156.
Liu, S.F., Mi, B.B., Fang, X.S., Li, X.Y., Pan, H.J., Chen, M.T., Shi, X.F., 2017. A preliminary study of a sediment core drilled from the mud area on the inner shelf of the East China Sea: Implications for paleoclimatic changes during the fast transgression period (13 ka B.P.–8 ka B.P.). Quat. Int. 441, 35–50.
Liu, J.T., Hsu, R.T., Yang, R.J., Wang, Y.P., Wu, H., Du, X., Li, A., Chien, S.C., Lee, J., Yang, S., Zhu, J., Su, C.-C., Chang, Y., Huh, C.-A., 2018a. A comprehensive sediment dynamics study of a major mud belt system on the inner shelf along an energetic coast. Sci. Rep. 8, 4229.
Liu, X.T., Li, A.C., Dong, J., Lu, J., Huang, J., Wan, S.M., 2018b. Provenance discrimination of sediments in the Zhejiang-Fujian mud belt, East China Sea: Implications for the development of the mud depocenter. J. Asian Earth Sci. 151, 1–15.
Liu, X.T., Li, A.C., Dong, J., Zhuang, G.C., Xu, F.J., Wan, S.M., 2018c. Nonevaporative origin for gypsum in mud sediments from the East China Sea shelf. Mar. Chem. 205, 90–97.
Loyd, S.J., Marenco, P.J., Hagadorn, J.W., Lyons, T.W., Kaufman, A.J., Sour-Tovar, F., Corsetti, F.A., 2012. Sustained low marine sulfate concentrations from the Neoproterozoic to the Cambrian: insights from carbonates of northwestern Mexico and eastern California. Earth Planet. Sci. Lett. 339–340, 79–94.
McKay, J.L., Longstaffe, F.J., 2003. Sulphur isotope geochemistry of pyrite from the Upper Cretaceous Marshybank Formation, Western Interior Basin. Sediment. Geol. 157, 175–195.
Nehlich, O., 2015. The application of sulphur isotope analyses in archaeological research: a review. Earth-Sci. Rev. 142, 1–17.
Pasquier, V., Sansjofre, P., Rabineau, M., Revillon, S., Houghton, J., Fike, D.A., 2017. Pyrite sulfur isotopes reveal glacial-interglacial environmental changes. Proc. Natl. Acad. Sci. U. S. A. 114, 5941–5945.
Passier, H.F., Middelburg, J.J., deLange, G.J., Bottcher, M.E., 1997. Pyrite contents, microtextures, and sulfur isotopes in relation to formation of the youngest eastern Mediterranean sapropel. Geology 25, 519–522.
Price, F.T., Shieh, Y.N., 1979. Fractionation of sulfur isotopes during laboratory synthesis of pyrite at low temperatures. Chem. Geol. 27, 245–253.
Raiswell, R., Buckley, F., Berner, R.A., Anderson, T., 1988. Degree of pyritization of iron as a paleoenvironmental indicator of bottom-water oxygenation. J. Sediment. Res. 58, 812–819.
Rees, C., 1973. A steady-state model for sulphur isotope fractionation in bacterial reduction processes. Geochim. Cosmochim. Acta 37, 1141–1162.
Riedinger, N., Pfeifer, K., Kasten, S., Garming, J.F.L., Vogt, C., Hensen, C., 2005. Diagenetic alteration of magnetic signals by anaerobic oxidation of methane related to a change in sedimentation rate. Geochim. Cosmochim. Acta 69, 4117–4126.
Riedinger, N., Brunner, B., Krastel, S., Arnold, G.L., Wehrmann, L.M., Formolo, M.J., Beck, A., Bates, S.M., Henkel, S., Kasten, S., Lyons, T.W., 2017. Sulfur cycling in an iron oxide-dominated, dynamic marine depositional system: the Argentine continental margin. Front. Earth Sci. 5.
Ries, J.B., Fike, D.A., Pratt, L.M., Lyons, T.W., Grotzinger, J.P., 2009. Superheavy pyrite ($\delta^{34}S_{pyr} > \delta^{34}S_{CAS}$) in the terminal Proterozoic Nama Group, southern Namibia: a consequence of low seawater sulfate at the dawn of animal life. Geology 37, 743–746.
Shang, S., Fan, D.D., Yin, P., Burr, G., Zhang, M.Y., Wang, Q., 2018. Late Quaternary environmental change in Oujiang delta along the northeastern Zhe-Min Uplift zone (Southeast China). Palaeogeogr. Palaeoclimatol. Palaeoecol. 492, 64–80.
Sim, M.S., Bosak, T., Ono, S., 2011a. Large sulfur isotope fractionation does not require disproportionation. Science 333, 74–77.
Sim, M.S., Ono, S., Donovan, K., Templer, S.P., Bosak, T., 2011b. Effect of electron donors on the fractionation of sulfur isotopes by a marine *Desulfovibrio* sp. Geochim. Cosmochim. Acta 75, 4244–4259.
Tostevin, R., Turchyn, A.V., Farquhar, J., Johnston, D.T., Eldridge, D.L., Bishop, J.K.B., McIlvin, M., 2014. Multiple sulfur isotope constraints on the modern sulfur cycle. Earth Planet. Sci. Lett. 396, 14–21.
Wilkin, R.T., Arthur, M.A., 2001. Variations in pyrite texture, sulfur isotope composition, and iron systematics in the Black Sea: evidence for Late Pleistocene to Holocene excursions of the O_2-H_2S redox transition. Geochim. Cosmochim. Acta 65, 1399–1416.
Wing, B.A., Halevy, I., 2014. Intracellular metabolite levels shape sulfur isotope fractionation during microbial sulfate respiration. Proc. Natl. Acad. Sci. U. S. A. 111, 18116–18125.
Wortmann, U.G., Bernasconi, S.M., Böttcher, M.E., 2001. Hypersulfidic deep biosphere indicates extreme sulfur isotope fractionation during single-step microbial sulfate reduction. Geology 29, 647–650.
Xu, F.J., Li, A.C., Xu, K.H., Li, T.G., Chen, S.Y., Wan, S.M., Liu, J.G., 2009. Cold event at 5500 a BP recorded in mud sediments on the inner shelf of the East China Sea. Chin. J. Oceanol. Limnol. 27, 975–984.
Xu, F.J., Li, A.C., Li, T.G., Xu, K.H., Chen, S.Y., Qiu, L.W., Cao, Y.C., 2011. Rare earth element geochemistry in the inner shelf of the East China Sea and its implication to sediment provenances. J. Rare Earths 29, 702–709.
Xu, K.H., Li, A.C., Liu, J.P., Milliman, J.D., Yang, Z.S., Liu, C.S., Kao, S.J., Wan, S.M., Xu, F.J., 2012. Provenance, structure, and formation of the mud wedge along inner continental shelf of the East China Sea: a synthesis of the Yangtze dispersal system. Mar. Geol. 291, 176–191.
Yang, S.Y., Wang, Z.B., Dou, Y.G., Shi, X.F., 2014. A review of sedimentation since the Last Glacial Maximum on the continental shelf of eastern China. Geol. Soc. Lond. Mem. 41, 293–303.
Yang, S.Y., Bi, L., Li, C., Wang, Z.B., Dou, Y.G., 2015. Major sinks of the Changjiang (Yangtze River)-derived sediments in the East China Sea during the late Quaternary. Geol. Soc. Lond., Spec. Publ. 429, 137–152.
Yao, P., Yu, Z.G., Bianchi, T.S., Guo, Z.G., Zhao, M.X., Knappy, C.S., Keely, B.J., Zhao, B., Zhang, T.T., Pan, H.H., Wang, J.P., Li, D., 2015. A multiproxy analysis of sedimentary organic carbon in the Changjiang Estuary and adjacent shelf. J. Geophys. Res. Biogeosci. 120, 1407–1429.
Zhao, B., Yao, P., Bianchi, T.S., Arellano, A.R., Wang, X.C., Yang, J.B., Su, R.G., Wang, J.P., Xu, Y.H., Huang, X.Y., Chen, L., Ye, J., Yu, Z.G., 2018. The remineralization of sedimentary organic carbon in different sedimentary regimes of the Yellow and East China Seas. Chem. Geol. 495, 104–117.
Zhu, M.X., Chen, K.K., Yang, G.P., Fan, D.J., Li, T., 2016. Sulfur and iron diagenesis in temperate unsteady sediments of the East China Sea inner shelf and a comparison with tropical mobile mud belts (MMBs). J. Geophys. Res. Biogeosci. 121, 2811–2828.